Scaling Laws for Advection Dominated Flows: Applications to Low Luminosity Galactic Nuclei.

Rohan Mahadevan
Harvard-Smithsonian Center for Astrophysics, 60 Garden St., Cambridge, MA 02138.

ABSTRACT

We present analytical scaling laws for self–similar advection dominated flows. The spectra from these systems range from $10^8 - 10^{20}$ Hz, and are determined by considering cooling of electrons through synchrotron, bremsstrahlung, and Compton processes. We show that the spectra can be quite accurately reproduced without detailed numerical calculations, and that there is a strong testable correlation between the radio and X-ray fluxes from these systems. We describe how different regions of the spectrum scale with the mass of the accreting black hole, M, the accretion rate of the gas, $\dot{M}$, and the equilibrium temperature of the electrons, T_e. We show that the universal radio spectral index of 1/3 observed in most elliptical galaxies (Slee et al. 1994) is a natural consequence of self–absorbed synchrotron radiation from these flows. We also give expressions for the total luminosity of these flows, and the critical accretion rate, $\dot{M}_{\rm crit}$, above which the advection solutions cease to exist. We find that for most cases of interest the equilibrium electron temperature is fairly insensitive to M, $\dot{M}$, and parameters in the model. We apply these results to low luminosity black holes in galactic nuclei. We show that the problem posed by Fabian & Canizares (1988) of whether bright elliptical galaxies host dead quasars is resolved, as pointed out recently by Fabian & Rees (1995), by considering advection–dominated flows.

1. Introduction.

The observational proof for the existence of black holes is one of the outstanding problems in astrophysics today. It is generally believed that black holes exist in binary star systems, at the centers of most normal galaxies, and are the central engines that power distant quasars. Attempts to prove the existence of these singularities are confined to inferring their presence by observing how they affect their environment. Measuring the kinematics of stellar systems and gas orbiting near the cores of galaxies (eg. van der Marel 1995a, b), using time variability arguments of the X–ray fluxes from quasars (eg. Wandel & Mushotzky 1986), or measuring the mass function in X-ray

binaries (eg. Haswell et al. 1993) are ways of inferring the existence of a massive object (black hole) that is confined to a small volume.

Another way of inferring the presence of a black hole is to consider the emission spectrum produced by an accretion disk as the surrounding gas accretes onto the central object. When considering black hole systems, the standard theory of accretion disks has serious difficulties in explaining the entire spectrum of these systems. The primary problem in the standard thin disk models is that the accreting gas is optically thick, and radiates locally as a modified black body spectrum (see Frank et al. 1992). This simple spectrum clearly falls short of explaining the entire emission from the radio to hard X-rays of these systems. Models have been proposed which explain the emission spectrum at certain frequencies (eg. Duschl & Lesch 1994), but these fail to explain the emission in other regions of the spectrum.

A possibility of explaining the entire spectrum of these systems has recently emerged with the consideration of advection–dominated accretion (Rees et al. 1982; Abramowicz et al. 1988; Narayan & Yi 1994, 1995a,b; Abramowicz et al. 1995). Unlike standard accretion disk theory, one class of advection–dominated accretion considers accretion flows that are optically thin and have low radiative efficiency. These flows have a two–temperature structure (Shapiro, Lightman, & Eardley 1976) and hence do not require all the viscously dissipated energy to be radiated locally, but instead allow a large fraction of the generated energy to be advected inwards, with the flow, to be ultimately deposited into the black hole. The total luminosity from these disks is therefore much lower, for a fixed accretion rate, than the luminosity from a thin accretion disk. It is however also possible to have a disk structure where there is an outer thin disk, which becomes advection–dominated as the flow approaches the black hole. In this case the outer disk gives the standard modified black body spectrum (Frank et al. 1992) which produces standard thin disk luminosities (eg. Narayan 1996; Narayan, Mc Clintock & Yi 1996, Lasota et al. 1996). For the present discussion we neglect the outer disk component since standard thin disks are well understood, and we are mainly interested in the advection–dominated flow.

The optically thin accretion flows in advection dominated systems naturally require electrons in the gas to cool via synchrotron, bremsstrahlung and inverse Compton processes. These processes are responsible for producing the entire spectrum, in these systems, from the radio to hard X-rays, in a natural way. A unique feature in considering advection flows to describe accreting black hole systems, is that they *require* the existence of an event horizon (Narayan, Yi, & Mahadevan 1996; Narayan, Mc Clintock, & Yi 1996), since a hard surface (eg. a neutron star) would re–radiate all the advected energy, thereby producing an equivalent total luminosity as predicted by a thin accretion disk. Successful application of these models to black hole systems might therefore prove the existence of an even horizon (Narayan, Yi, & Mahadevan 1995; Narayan, Mc Clintock, & Yi 1996).

Detailed numerical calculations which consider the individual cooling and heating processes in the flow have been performed by Narayan & Yi (1995b), and the resulting spectra have been successfully applied to a number of putative black hole systems (eg. Narayan et al. 1995, Lasota et al. 1996, Narayan, Mc Clintock, & Yi 1996). Narayan & Yi (1995b) have numerically obtained a number of interesting properties of these advection flows. From the detailed calculations, however, it is difficult to deduce how different regions of a spectrum scale as quantities such as the mass of the central object and accretion rate are varied.

The present paper develops analytical expressions to describe the general properties of advection dominated flows. We deduce scaling laws which give physical insight to the detail processes involved, and show how these simple laws give rise to quite an accurate description of these flows. In §2. we review the self–similar flow equations for advection dominated disks. §3. describes the heating and cooling processes, and §4. shows how the entire spectrum from these systems can be understood by simple scaling laws. §5. addresses the general properties of the flow. In §6. we follow Fabian & Rees (1995) and apply the results to resolve the long standing problem posed by Fabian & Canizares (1988) of whether elliptical galaxies host dead quasars. Finally, in §7., we discuss future applications of these models and conclude.

2. Self-Similar Flow Equations.

In this section we review some of the basic assumptions and equations of the self–similar advection dominated models developed by Narayan & Yi (1995b). Narayan & Yi (1995b) present self–similar equations which describe local properties of the accreting gas as a function of the mass, M, the accretion rate, $\dot{M}$, the radius, R, the viscosity parameter, α, the ratio of gas pressure to total pressure, β, and the fraction of viscously dissipated energy that is advected, f.

The accreting gas in an advection–dominated flow is a two temperature optically thin plasma. The ions are at their virial temperature and the electrons are significantly cooler. The total pressure, p, in these flows is the sum of gas (p_g) and magnetic (p_m) pressure. The gas is roughly in equipartition with an isotropically tangled magnetic field, B, which contributes a factor $1-\beta$ to the total pressure,

$$p_m \equiv (1-\beta)\rho c_s^2 = \frac{B^2}{24\,\pi}. \tag{1}$$

This equation differs from Narayan & Yi (1995) by a factor of 1/3 to account for the pressure due to a three dimensional tangled magnetic field. ρ and c_s are the mass density and speed of sound.

The self–similar equations are written in terms of scaled quantities: the mass is scaled in solar mass units

$$M = m\, M_{\odot}, \tag{2}$$

the radius in Schwarzschild radii

$$R = r R_{\rm Schw}, \qquad R_{\rm Schw} = \frac{2GM}{c^2} = 2.95 \times 10^5\, m \ \ {\rm cm}, \tag{3}$$

and the accretion rate in Eddington units

$$\dot{M} = \dot{m}\, \dot{M}_{\rm Edd},$$

$$\dot{M}_{\rm Edd} = \frac{L_{\rm Edd}}{\eta_{\rm eff} c^2} = 1.39 \times 10^{18} m \ \ {\rm g\ s^{-1}}, \tag{4}$$

where $\eta_{\rm eff} = 0.1$ is the standard efficiency in converting matter to energy (Frank et al. 1992).

Since these flows are essentially spherical in geometry (Narayan & Yi 1995b), the vertical scale height of the disk is set equal to the radius in the equations that follow. With this approximation and the scalings above, the self–similar equations for the accretion flow which are relevant for the present discussion are (Narayan & Yi 1995b):

$$\begin{aligned}
\rho &= 6.00 \times 10^{-5}\ \alpha^{-1} c_1^{-1}\, m^{-1}\, \dot{m}\, r^{-3/2} \ \ {\rm g\ cm^{-3}}, \\
B &= s_1\, m^{-1/2}\, \dot{m}^{1/2}\, r^{-5/4} \ \ {\rm G}, \\
n_e &= b_1\, m^{-1}\, \dot{m}\, r^{-3/2} \ \ {\rm cm^{-3}}, \\
s_1 &= 1.42 \times 10^9\, \alpha^{-1/2} (1-\beta)^{1/2} c_1^{-1/2} c_3^{1/2}, \\
b_1 &= 3.16 \times 10^{19}\, \alpha^{-1}\, c_1^{-1}.
\end{aligned} \tag{5}$$

These are the equations that differ from Narayan & Yi (1995b) since we have assumed spherical accretion. n_e is the numberdensity of electrons, and c_1, c_3 are constants as defined in Narayan & Yi (1995b). [1] For all cases of interest, $c_1 \simeq 0.5$ and $c_3 \simeq 0.3$.

---

[1] In the definition of c_1, c_3 as given in Narayan & Yi (1995b), the ratio of specific heats of the gas is different from the present paper. We use (Esin 1996)

$$\gamma = \frac{8-3\beta}{6-3\beta}.$$

3. Energy Balance and Heating of a Two Temperature Plasma.

The accreting gas in the advection flows are heated locally by viscous forces. In the analysis of Narayan & Yi (1995b), the viscously dissipated energy q^+ is mainly transferred to the ions in the gas. A fraction f of this energy is carried inwards by the accreting gas, while the remaining fraction $1 - f$ is transferred from the ions to the electrons to be radiated via synchrotron, inverse Compton and bremsstrahlung emission. There are therefore two energy equations that need to be satisfied. In the present analysis we account for the possibility of viscously heating the electrons by a fraction δ. Since the heat generated by the viscous forces is transferred mainly to those particles with more inertial mass, we would expect that the fraction δ of viscous energy transferred to the electrons is in the ratio of the electron to ion mass $\sim m_e/m_i \sim 1/2000$. The energy balance for the ions therefore satisfies

$$\begin{aligned} q^+ &= f\, q^+ + q^{ie} + \delta\, q^+, \\ &\equiv q^{\rm adv} + q^{\rm e+}, \quad \text{ergs s}^{-1}\ \text{cm}^{-3}, \end{aligned} \tag{6}$$

with

$$q^{\rm adv} \equiv f\, q^+,$$
$$q^{\rm e+} \equiv q^{ie} + \delta\, q^+.$$

Here, q^+ and q^{ie} are the rate of heating per unit volume and rate of transfer of energy from the ions to the electrons per unit volume respectively, $q^{\rm adv}$ is the advected energy, and $q^{\rm e+}$ is total electron heating rate including viscous heating.

The electrons satisfy the energy equation, $q^{\rm e+} = q^-$, where q^- is the sum of all the local cooling processes (synchrotron, bremsstrahlung, and inverse Compton). Setting $\delta = 0$ in these equations gives the energy equations of Narayan & Yi (1995b). For a given m, $\dot{m}$, r, α, and β, the electron and ion energy equations are solved to determine the electron and ion temperatures of the plasma, and to determine the fraction f of advected energy. Narayan & Yi (1995b) use detailed numerical methods to solve these equations at each radius r, in order to determine the local properties of the flow and the spectrum that is produced. We obtain similar results with less effort analytically.

For the present analysis, the quantities of interest are the volume integrated quantities, Q^+, $Q^{\rm e+}$, Q^-, which are obtained by integrating q^+, $q^{\rm e+}$, q^- throughout the volume of the advection region. Using scaled quantities, and the approximation $H = R$, the volume integrated quantities are defined by

$$\begin{aligned} Q^X &= \int_{R_{min}}^{R_{max}} 4\pi\, R^2\, q^X\, dR, \\ &= 3.23 \times 10^{17}\, m^3 \int_{r_{\rm min}}^{r_{\rm max}} q^X\, r^2\, dr \quad \text{ergs s}^{-1}, \end{aligned} \tag{7}$$

where X denotes any quantity of interest. The lower limit is taken to be $r_{\rm min} = 3$ since the self–similar solutions break down for $r \lesssim$few (Mastsumoto et al. 1985, Narayan 1996). This choice of $r_{\rm min}$ is also in accordance with previous calculations (eg. Narayan et al. 1995, Lasota et al. 1996), and we find that this reproduces the detailed spectra quite well. To determine the upper limit, we use some of the properties of the flow developed by Narayan & Yi (1995b). Narayan & Yi (1995b) have shown that for $r \gtrsim 10^3$, the flow becomes a cool $\sim 10^{8.5}$ K one temperature plasma, and not much radiation is produced, while for $r < 10^3$ the electron temperature is fairly constant while the ion temperature increases as $1/r$. Since most of the radiation from these flows originate at $r < 10^3$, where the $T_e \gtrsim 10^9$, and the present discussion is interested in the radiation produced from such a flow, we set $r_{\rm max} = 10^3$. In the discussion that follows, we assume that the electron temperature is constant for $r < 10^3$, as suggested by the detailed calculations of Narayan & Yi (1995b). The energy balance equations take the form

$$\begin{aligned} Q^+ &= Q^{\rm adv} + Q^{\rm e+}, \\ Q^{\rm e+} &= Q^{ie} + \delta\, Q^+, \\ Q^{\rm e+} &= Q^-, \\ Q^- &= P_{\rm synch} + P_{\rm Compton} + P_{\rm brems}, \end{aligned} \tag{8}$$

where $P_{\rm synch}$, $P_{\rm Compton}$, $P_{\rm brems}$ are the total cooling rates for the individual processes. The energy equations for the ions and electrons are solved self–consistently to determine the fraction of the advected energy f, and the electron temperature T_e. To do this, we first give analytic equations for the heating terms Q^+, Q^{ie}, and in the next section determine the cooling terms $P_{\rm synch}$, $P_{\rm Compton}$, $P_{\rm brems}$, and the spectra they produce.

3.1. Heating Processes: Ion Heating

The ions are heated by viscous forces. The total heating rate, Q^+, is obtained by using eq.(7) and integrating q^+, as defined in Narayan & Yi (1995b), throughout the advection region. This gives

$$Q^+ = 9.39 \times 10^{38}\ \frac{1-\beta}{f}\, c_3\, m\, \dot{m}\, r_{\rm min}^{-1}\ \ {\rm ergs\ s^{-1}}, \tag{9}$$

where we have set $r_{\rm max} \gg r_{\rm min}$. For low values of α, c_3 is independent of α, and eq. (9) shows that for fixed m and $\dot{m}$, the heating rate depends only on the fraction of gas to magnetic pressure.

3.2. Heating Processes: Electron Heating.

The electrons are heated by two processes: by viscous heating $\delta\, Q^+$, where an expression for Q^+ has been derived above, and by a transfer of energy from the ions to electrons via Coulomb interactions. The heating rate per unit volume due to Coulomb interactions is given by Stepney & Guilbert (1983), Narayan & Yi (1995b), and can be approximated to (see Appendix A.)

$$q^{ie} \simeq 5.61 \times 10^{-32}\,(T_i - T_e)\, b_1^2\, m^{-2}\, \dot{m}^2\, r^{-3}\, r^{-1}\, g(\theta_e) \;\; \text{ergs cm}^{-3}\ \text{s}^{-1}, \tag{10}$$

where we have substituted for n_e, $\theta_e = kT_e/m_e c^2$, and

$$g(\theta_e) \equiv \frac{1}{K_2(1/\theta_e)} \left(2 + 2\theta_e + \frac{1}{\theta_e}\right) e^{-1/\theta_e}, \tag{11}$$

which is tabulated for various values of temperature in Table 1. From Narayan & Yi (1995b), the ion temperature can be approximated to

$$\begin{aligned} T_i &= 6.66 \times 10^{12} \beta c_3 r^{-1} - 1.08 T_e, \\ &\simeq h\, r^{-1}, \end{aligned} \tag{12}$$

where

$$h = 6.66 \times 10^{12} \beta c_3.$$

The the second term in eq.(12) has been neglected compared with the first since the electron temperatures are considerably lower that the ion temperatures for $r \lesssim 10^3$.

The total ion–electron heating rate for the electrons is (cf. eq. 7)

$$Q^{ie} \simeq 1.2 \times 10^{38}\, g(\theta_e)\, \alpha^{-2}\, c_1^{-2}\, c_3\, \beta\, m\, \dot{m}^2\, r_{\rm min}^{-1} \;\text{ergs s}^{-1}, \tag{13}$$

where we have substituted for b_1, h, and assumed $r_{\rm max} \gg r_{\rm min}$. Combining the equations above, the total heating of the electrons is given by

$$\begin{aligned} Q^{\rm e+} &= Q^{ie} + \delta\, Q^+, \\ &\simeq 1.2 \times 10^{38}\, g(\theta_e)\, \alpha^{-2}\, c_1^{-2}\, c_3\, \beta\, m\, \dot{m}^2\, r_{\rm min}^{-1} \\ &+ \delta\, 9.39 \times 10^{38}\, \epsilon'\, c_3\, m\, \dot{m}\, r_{min}^{-1}. \end{aligned} \tag{14}$$

The major source for electron heating depends on the value of $\dot{m}$; for high $\dot{m}$, $Q^{ie} \gg \delta\, Q^+$, whereas for low $\dot{m}$, $\delta\, Q^+ \gg Q^{ie}$. By setting $Q^{ie} = \delta\, Q^+$, we can determine the transition accretion rate:

$$\dot{m} \sim 8.8 \times 10^{-5} \left(\frac{\alpha}{0.3}\right)^2 \left(\frac{\delta}{2000^{-1}}\right) \left(\frac{1-\beta}{0.5}\right) \left(\frac{\beta}{0.5}\right)^{-1} \left(\frac{c_1}{0.5}\right)^2 \left(\frac{f}{1.0}\right)^{-1} g(\theta_e)^{-1}. \tag{15}$$

4. Energy Balance: Cooling Processes and the Components of the Spectrum

In order to balance the viscous and Coulomb heating, the electrons cool through three distinct processes: synchrotron, bremsstrahlung, and inverse Compton emission. The emission in different regions of the spectrum is determined by these individual cooling processes. Synchrotron radiation is responsible for the radio to sub-millimeter emission, while a combination of bremsstrahlung emission and inverse Compton scattering of synchrotron photons is responsible for the sub-millimeter to X-ray emission. This is one of the successes of the advection-dominated models: explaining, using few free parameters, the entire spectra of accreting systems. A natural question to ask is how does the amount of emission and shape of the final spectrum depend on variables like α, β, m, $\dot{m}$, and T_e ? Previous papers (eg. Narayan & Yi 1995b; Narayan, McClintock, & Yi 1996) have used detailed numerical calculations to evaluate the spectrum produced. The analysis presented here give less detailed spectra, but is much faster in determining the general characteristics, and the individual components of the spectra produced.

In the analysis that follows, the spectrum is divided into three components. The cyclo-synchrotron component, and the bremsstrahlung and the inverse Compton component. Fig. 1 shows representative plots of the spectrum for a fixed mass $m = 5 \times 10^9$, and for different accretion rates $\dot{m} = (3, 6, 12, 24) \times 10^{-4}$, with $\alpha = 0.3$, and $\beta = 0.5$. For one curve, the individual components of the spectrum have been labeled as S for synchrotron, B for bremsstrahlung, and C for comptonization. In the sub–sections below each of these components are describe with the appropriate analytic approximations.

4.1. Cyclo-Synchrotron Emission and the Radio-Sub-mm Spectrum.

The radio to sub-mm spectrum is defined by three quantities: 1) the luminosity of the radio spectrum, 2) the maximum (peak) frequency beyond which the spectrum falls off exponentially, and 3) the slope of the radio spectrum. We treat each of these separately.

In the optically thin limit, the spectrum of cyclo–synchrotron radiation by an isotropic distribution of relativistic thermal electrons is given by (Mahadevan et al. 1996, Narayan & Yi 1995b)

$$\epsilon_{\rm synch} d\nu = 4.43 \times 10^{-30} \frac{4\pi\, n_e\, \nu}{K_2(1/\theta_e)}\, M(x_M), \tag{16}$$

where we use the extreme relativistic expression for $M(x_M)$ given by

$$M(x_M) = \frac{4.0505}{x_M^{1/6}} \left(1 + \frac{0.40}{x_M^{1/4}} + \frac{0.5316}{x_M^{1/2}}\right) \exp\left(-1.8899 x_M^{1/3}\right), \tag{17}$$

and

$$x_M \equiv \frac{2\nu}{3\nu_b \theta_e^2}, \qquad \nu_b \equiv \frac{eB}{2\pi\, m_e\, c}. \tag{18}$$

The cyclo–synchrotron photons in these plasmas are self-absorbed, and give a black body spectrum, up to a critical frequency ν_c. The frequency at which this occurs, at each radius r, is determined by evaluating the total cyclo-synchrotron emission over a volume of radius r, and equating it to the Raleigh-Jeans black body emission from the surface of this sphere. This gives the condition

$$4.43 \times 10^{-30} \frac{4\pi\, n_e\, \nu_c}{K_2(1/\theta_e)}\, M(x_M)\, \frac{4\pi}{3} R^3 = \pi 2 \frac{\nu_c^2}{c^2}\, kT_e\, 4\pi\, R^2 \tag{19}$$

which can be rewritten in terms of x_M as

$$\exp\left(1.8899\, x_M^{1/3}\right) = 2.49 \times 10^{-10}\ \frac{4\pi\, n_e\, R}{B}\ \frac{1}{\theta_e^3\, K_2(1/\theta_e)} \left(\frac{1}{x_M^{7/6}} + \frac{0.40}{x_M^{17/12}} + \frac{0.5316}{x_M^{5/3}}\right). \tag{20}$$

x_M is determined in Appendix B.. Given x_M, the cutoff frequency at each radius is determined by eqs.(18) to be

$$\begin{aligned} \nu_c &= \frac{3}{2}\, \theta_e^2\, \nu_b\, x_M, \\ &= s_1\, s_2\, m^{-1/2}\, \dot{m}^{1/2}\, T_e^2\, r^{-5/4}, \quad \text{Hz}, \end{aligned} \tag{21}$$

where s_1 is given in eqs. (5) and

$$s_2 \equiv 1.19 \times 10^{-13}\, x_M, \tag{22}$$

At this frequency the radiation becomes optically thin and the luminosity is given by the Raleigh-Jeans part of the black body spectrum

$$\begin{aligned} L_{\nu_c} &= \pi\, 2\, \frac{\nu_c^2}{c^2}\, k\, T_e\, 4\pi\, R^2, \\ &= s_3\, T_e\, \nu_c^2\, m^2\, r^2 \ \ \text{ergs s}^{-1}\ \text{Hz}^{-1}, \qquad s_3 = 1.05 \times 10^{-24}. \end{aligned} \tag{23}$$

This determines the luminosity at each point along the radio spectrum.

For a fixed T_e, eq.(21) shows how the cutoff frequency varies with r. Emission observed at higher frequencies originates at smaller radii, closer to the central black hole. The peak frequency, and the power at that frequency are determined by setting $r = r_{\rm min}$ in eqs.(21),(23),

$$\nu_p = s_1\, s_2\, m^{-1/2}\, \dot{m}^{1/2}\, T_e^2\, r_{\rm min}^{-5/4} \ \ \text{Hz},$$

$$\nu_p L_{\nu_p} = s_1^3\, s_2^3\, s_3\, r_{\rm min}^{-7/4}\, m^{1/2}\, \dot{m}^{3/2}\, T_e^7 \;\; {\rm ergs\ s^{-1}}, \tag{24}$$

which shows that the luminosity at the peak frequency is very sensitive to the electron temperature.

The slope of the radio spectrum is a direct consequence of x_M and T_e being essentially constant, and the the Raleigh–Jeans part of the black body spectrum. Since $B \propto r^{-5/4}$, eq.(21) shows that $r \propto \nu_c^{-4/5}$. From eq.(23), $L_\nu \propto \nu_c^2 r^2 \propto \nu_c^{2/5}$. The complete spectrum is obtained by rewriting eq.(21) in terms of r and substituting in eq.(23) to give

$$L_\nu \simeq s_3\, (s_1 s_2)^{8/5}\; m^{6/5} \dot{m}^{4/5}\, T_e^{21/5}\, \nu^{2/5} \;\; {\rm ergs\ s^{-1}\ Hz^{-1}}. \tag{25}$$

This produces a spectrum with slope of 2/5, which is similar to the slope of 1/3 produced by optically thin synchrotron emission (the dependence of x_M on r is not taken into account here, numerically, $x_M \sim r^{1/15}$ which makes L_ν even closer to $\sim \nu^{1/3}$). The advection–dominated models therefore give a very natural explanation to the characteristic 1/3 radio spectral indices observed when looking at putative black hole systems (Wrobel 1991; Slee et al. 1994; Narayan et al. 1995). The 2/5 spectral slope extends from ν_p down to $\nu_{\rm min}$ where $\nu_{\rm min}$ is the cutoff frequency given by setting $r = r_{\rm max}$ in eq.(21) (cf. Fig. 1). This is is a direct consequence of the advection flows having a constant electron temperature for $r \lesssim 10^3$. Beyond this radius the advection flows become a one temperature plasma and $T_e \propto r^{-1}$, which gives a steeper radio slope of 22/13, as long as $T_e \gtrsim 10^8$K (below this temperature there is no synchrotron radiation).

We assume that $\nu_{\rm min} \ll \nu_p$ and obtain the total power from

$$\begin{aligned} P_{\rm synch} &= \int_0^{\nu_p} L_\nu\, d\nu \simeq 0.71\, \nu_p\, L_{\nu_p}, \\ &\simeq 5.3 \times 10^{35} \left(\frac{x_M}{1000}\right)^3 \left(\frac{\alpha}{0.3}\right)^{-3/2} \left(\frac{1-\beta}{0.5}\right)^{3/2} \left(\frac{c_1}{0.5}\right)^{-3/2} \\ &\times \left(\frac{c_3}{0.3}\right)^{3/2} \left(\frac{r_{\rm min}}{3}\right)^{-7/4} \left(\frac{T_e}{10^9}\right)^7 m^{1/2}\, \dot{m}^{3/2} \;\; {\rm ergs\ s^{-1}}. \end{aligned} \tag{26}$$

In this simple description, the synchrotron spectrum is assumed to terminate at ν_p (cf. Fig. 1) and does not reproduce the exponential decay in the emission that is expected from thermal plasmas (Mahadevan et al. 1996). This is because, in this simple discussion, we have assumed that all the photons to be comptonized occur at the peak frequency (see below), and so the comptonized spectrum begins at ν_p.

4.2. Bremsstrahlung Emission: The Sub-mm to Hard X-ray Spectrum.

Bremsstrahlung emission is characterized by a constant luminosity L_ν, up to a frequency $h\nu = k\,T_e$ where the spectrum turns and falls off exponentially (cf. Fig. 1). The total emission due to bremsstrahlung radiation is given by eq. (7) with $q^X = q_{\rm brems}$, where $q_{\rm brems}$ is the bremsstrahlung emission per unit volume due to both electron-electron and electron-ion interactions. The bremsstrahlung emission per unit volume is given by (Stepney & Guilbert 1983; Narayan & Yi 1995b),

$$\begin{aligned} q_{\rm brems} &= q_{ei} + q_{ee}, \\ &\simeq 1.48 \times 10^{-22}\, n_e^2\, F(\theta_e), \quad {\rm ergs\ cm^{-3}\ s^{-1}}, \end{aligned} \tag{27}$$

which represent the contributions from electron–electron and electron–ion interactions, and

$$F(\theta_e) = \begin{cases} 4\left(\dfrac{2\theta_e}{\pi^3}\right)^{1/2}(1+1.781\,\theta_e^{1.34}) + 1.73\,\theta_e^{3/2}(1+1.1\,\theta_e+\theta_e^2-1.25\,\theta_e^{5/2}), & \theta_e < 1, \\ \\ \left(\dfrac{9\theta_e}{2\pi}\right)[\ln(1.123\,\theta_e+0.48)+1.5] + 2.30\,\theta_e(\ln 1.123\,\theta_e + 1.28), & \theta_e > 1, \end{cases} \tag{28}$$

Using the expression for the number density, the total bremsstrahlung power is

$$P_{\rm brems} = 4.78 \times 10^{34}\, \alpha^{-2}\, c_1^{-2}\, \ln(r_{\rm max}/r_{\rm min})\, F(\theta_e)\, m\, \dot{m}^2, \tag{29}$$

and the spectrum due to bremsstrahlung emission is

$$\begin{aligned} L_{\rm brems}(\nu) &\simeq 2.29 \times 10^{24}\ \alpha^{-2}\, c_1^{-2}\, \ln(r_{\rm max}/r_{\rm min}) \\ &\times\ F(\theta_e)\, T_e^{-1}\, e^{-h\,\nu/k\,T_e}\, m\, \dot{m}^2 \quad {\rm ergs\ s^{-1}\ Hz^{-1}}, \end{aligned} \tag{30}$$

which is shown in Fig. 1. Comparing eq. (29) with eq. (26) shows that for most cases of interest, $P_{\rm brems} < P_{\rm synch}$, and can be neglected when considering the total cooling rate of the flow. However, when considering the entire emission spectrum, bremsstrahlung emission is important since it contributes to the X-ray emission.

4.3. Comptonization: The Sub-mm to Hard X-ray Spectrum.

In this discussion, we neglect the comptonization of bremsstrahlung emission, and only consider the comptonization of the soft cyclo–synchrotron photons. This is the other process responsible for the sub-mm to hard x-ray spectrum. The spectrum is defined by three quantities: 1) the initial frequency of the photons that are comptonized, 2) the maximum final frequency of a comptonized photon, and 3) the slope, α_c, of the comptonized spectrum (cf. Fig. 1).

The photons that are comptonized are the soft cyclo–synchrotron photons in the radio spectrum. The emission in the radio spectrum mainly occurs at the peak frequency, ν_p, and so we can make the approximation that all the synchrotron photons to be comptonized have an initial frequency of ν_p. The maximum final frequency of a comptonized photon is $h\nu_f = 3\,k\,T_e$, which is the average energy of a photon for saturated comptonization in the Wien regime.

The optical depth to electron scattering, τ_{es}, and how much a photon is amplified in one scattering, are the two quantities that determine the slope of the Compton spectrum. Photons at different radii see different optical depths, with photons at small radii seeing large optical depths and those at large radii seeing small optical depths. In this simple treatment we expect, on the average, that all the photons would probably see half the total optical depth. We therefore take the optical depth to electron scattering to be half of that as given in Narayan & Yi (1995b),

$$\begin{aligned} \tau_{es} &= 6.2\,\alpha^{-1}\,c_1^{-1}\,\dot{m}\,r^{-1/2}, \\ &= (23.87\,\dot{m})\left(\frac{\alpha}{0.3}\right)^{-1}\left(\frac{c_1}{0.5}\right)^{-1}\left(\frac{r_{\rm min}}{3}\right)^{-1/2}. \end{aligned} \tag{31}$$

We find that this choice of τ_{es} reproduces the more detailed comptonized spectrum quite well (Narayan, private communication).

In the standard treatment of comptonization (e.g. Rybicki & Lightman 1979, Dermer, Liang, & Canfield 1991), a photon with initial energy ϵ_i that undergoes k scatterings, has final energy $\epsilon_f \simeq A^k\,\epsilon_i$, where A is the mean amplifaction factor in one scattering which for thermal plasmas is

$$A = 1 + 4\,\theta_e + 16\,\theta_e^2. \tag{32}$$

For temperature ranges of interest, $2 < A < 50$. The luminosity of the emerging photons at frequency ν_f has the power–law shape

$$L_{\nu_f} \simeq L_{\nu_i}\left(\frac{\nu_f}{\nu_i}\right)^{-\alpha_c}, \tag{33}$$

where

$$\alpha_c \equiv \frac{-\ln\tau_{es}}{\ln A}. \tag{34}$$

The total Compton power is

$$\begin{aligned} P_{\rm Compton} &= \int_{\nu_p}^{3\,k\,T_e/h} L_{\nu_f}\,d\nu_f, \\ &= \frac{\nu_p\,L_{\nu_p}}{1-\alpha_c}\left[\left(\frac{6.2\times 10^7\,(T_e/10^9)}{(\nu_p/10^{12})}\right)^{1-\alpha_c} - 1\right] \ \text{ergs s}^{-1}. \end{aligned} \tag{35}$$

Eqs. (33), (34), and (35) show how the Compton power depends on the optical depth and temperature through the slope of the spectrum α_c. If $\alpha_c \gg 1$, comptonization can

be neglected. If $\alpha_c \lesssim 1$ then there is significant comptonization of the cyclo–synchrotron photons, and the cooling is dominated by the inverse Compton losses. The actual determination of α_c is done self–consistently and is discussed in §5.. Although eq. (35) is used to determine the total Compton power in the subsequent sections (see §5.), it is instructive to analytically approximate eq. (35) for $\alpha_c \gg 1$, and $\alpha_c < 1$, to determine how the Compton power scales in these regimes. We consider these two cases below, and show how the value of α_c determines whether the comptonization of the soft–cyclosynchrotron photons dominates over bremsstrahlung emission in the sub-mm to X-ray region of the spectrum.

4.3.1. $\alpha_c > 1$: Low Compton Cooling.

For $\alpha_c > 1$, the first term in the square brackets in eq. (35) can be neglected which gives

$$P_{\rm Compton}(\alpha_c > 1) \simeq \frac{\nu_p \, L_{\nu_p}}{\alpha_c - 1}, \tag{36}$$

with $\alpha_c \gg 1$ corresponding to no comptonization. Comparing this with eq.(26), the total Compton power is proportional to the total synchrotron power. If $\alpha_c \gg 1$, then the Compton power is less than the synchrotron power, and can be neglected when determining the total cooling rate. When $1 < \alpha_c < 2$, however, the Compton power is greater than the synchrotron power and contributes comparably to the total cooling rate.

4.3.2. $\alpha_c < 1$: Significant Compton Cooling.

For $\alpha_c < 1$, the second term in square brackets in eq. (35) can be neglected which gives

$$P_{\rm Compton}(\alpha_c < 1) \simeq \left(\frac{6.2 \times 10^7 \, (T_e/10^9)}{\nu_p/10^{12}} \right)^{1-\alpha_c} \frac{\nu_p \, L_{\nu_p}}{1 - \alpha_c}. \tag{37}$$

In this regime the Compton power dominates the total synchrotron power. The Compton power when $\alpha_c = 1$ is obtained by taking the limit as $\alpha_c \to 1$ of eq.(35).

4.3.3. Compton Luminosity.

The luminosity in the sub-mm to X-rays due to comptonization is

$$L_{\rm Compton} \simeq \nu_p^{\alpha_c} \, L_{\rm synch}(\nu_p) \, \nu^{-\alpha_c} \;\; {\rm ergs \; s^{-1} \; Hz^{-1}}, \tag{38}$$

and is sensitive to whether α_c is less than, equal to, or greater than 1. For $\alpha_c \gg 1$, the bremsstrahlung luminosity in the sub-mm to X-rays is greater than the Compton luminosity. When $\alpha_c < 1$ comptonization dominates the sub-mm to X-ray spectrum, and when $1 < \alpha_c < 2$ both bremsstrahlung and comptonization are dominant. Fig. 1 shows how an increase in the accretion rate increases the slope of the Compton spectrum. At low $\dot{m}$ the bremsstrahlung emission dominates the X-ray emission, when $\alpha_c > 1$, whereas for high $\dot{m}$, $\alpha_c < 1$, and the comptonized spectrum dominates the X-ray emission. α_c therefore determines the dominant source of emission at these frequencies. Note that in this simple description of comptonization, the spectrum begins from $\nu = \nu_p$ (cf. Fig 1) and therefore does not reproduce the characteristic dip in the spectrum between radio and sub-millimeter wavelengths (eg. Narayan et al. 1995). A more detailed Compton calculation would be needed for this.

5. General Properties of the Flow.

In the following sections, we use the results obtained to determine general properties of the advection–dominated flow. We first determine the temperature of the gas and α_c, then the total luminosity from the flow, and finally the critical accretion rate $\dot{m}_{\rm crit}$ above which the advection solution does not exist.

5.1. Equilibrium Temperatures and α_c.

Since the electrons are responsible for cooling, the temperature in these flows is determined by the energy balance equation for the electrons. The sum of the individual cooling processes are equated to the total heating of the electrons, and this equation is solved self–consistently for the temperature. We first determine the equilibrium temperature and α_c through simple numerical methods, and then provide analytic approximations which determine them.

5.1.1. Numerical Method.

For a given m, $\dot{m}$, α, and β, the total heating of the electrons is equated to the individual cooling processes, $Q^{e+} = P_{\rm synch} + P_{\rm brems} + P_{\rm Compton}$, and the electron temperature is varied until this equality is satisfied. At each value of T_e, the slope of the comptonized spectrum is determined through eq.(34). Solving for the electron temperature therefore fixes the slope of the comptonized spectrum. Fig. 2 shows numerical plots of the equilibrium temperature as a function of $\dot{m}$ for different values of the black hole mass m. Here, $\alpha = 0.3$, $\beta = 0.5$, and $\delta = 1/2000$. The corresponding values of x_M at each $\dot{m}$ is also shown. At high $\dot{m}$, the equilibrium temperatures are independent of m and are constant at a value $T_e \simeq 2.0 \times 10^9$. Further, at low $\dot{m}$, T_e increases with decreasing $\dot{m}$. Note however that if $\delta = 0$ then eq. (C17) shows that the temperature decreases as $\dot{m}$ decreases. This is because synchrotron cooling is the dominant source of cooling, and is much more efficient than the Coulomb heating at low $\dot{m}$.

Fig 3. shows the value of $1 - \alpha_c$, the slope of the spectrum on a $\nu\, L_\nu$ plot, as a function of $\dot{m}$, for different values of the central mass m. These correspond to the equilibrium conditions as shown in Fig. 2. At low $\dot{m}$, α_c becomes constant which is expected since both $\ln A$, $\ln \tau_{es} \propto \ln \dot{m}$. The value of this constant depends on the mass of the central black hole. At high accretion rates $\alpha_c \sim 0.5$

5.1.2. Analytic Determination.

An analytic determination of the equilibrium electron temperature allows an understanding of how it scales with different quantities in these models. To simplify the equations that follow, note that eqs.(26), (29), and (35) show that $P_{\rm brems} < P_{\rm synch}$, and that depending on the value of α_c, $P_{\rm synch}$ can be greater or less than $P_{\rm Compton}$. Further, since $P_{\rm brems}$ is very insensitive to the electron temperature ($\propto F(\theta_e)$), as compared with ($P_{\rm synch} + P_{\rm Compton} \propto T_e^7$), we find that for all ranges of m, $\dot{m}$, the contribution to the total cooling by bremmstrahlung emission, is negligible compared with synchrotron and Compton cooling, at the equilibrium temperatures. We therefore neglect bremmstrahlung cooling in the analysis that follows.

A rough estimate of α_c, for a given $\dot{m}$, can be obtained from eqs.(31) and (34). Using the range of temperatures of interest ($10^9 \leq T_e \leq 2 \times 10^{10}$) to determine the maximum and minimum values of $\ln A$, and setting $\alpha_c = 1$, eqs. (34), (31) show that if $\dot{m} \lesssim 10^{-4}\alpha$, then $\alpha_c \gtrsim 1$, and if $\dot{m} \geq 3 \times 10^{-3}\alpha$ then $\alpha_c \leq 1$. However for $10^{-4}\alpha \leq \dot{m} \leq 10^{-2}\alpha$ the value of α_c can be either greater or less than 1, depending on the temperature which has to be solved self-consistently. We consider the two cases.

$\underline{\alpha_c > 1.}$

In this limit synchrotron and Compton emission are the dominant sources of cooling,

and depending on the value of α_c Compton cooling is comparable to or less than the total synchrotron cooling (cf. §4.3.1.). Bremsstrahlung cooling is neglected. The total cooling rate is given by

$$\begin{aligned} Q^{-} &\simeq \left(0.71 + \frac{1}{\alpha_c - 1}\right) \nu_p \, L_{\nu_p} \\ &\simeq A_c \, \nu_p \, L_{\nu_p}, \end{aligned} \tag{39}$$

where the first term is due to synchrotron cooling and the second is due to Compton cooling (for $\alpha_c \gg 1$ we only consider synchrotron cooling and $A_c = 0.71$). This has to be equal to the total heating $Q^{\rm e+}$. However when $\alpha_c > 1$ and $\dot{m} < 10^{-3}\,\alpha^2$, from eq.(15) this is when Q^{ie} can be neglected compared with $\delta\, Q^{+}$ (see Appendix C. for the case $\delta = 0$). Setting $\delta\, Q^{+} = Q^{-}$, and rearranging terms gives

$$\begin{aligned} T_e &= \frac{1.1 \times 10^9}{A_c^{1/7}} \left(\frac{\delta}{2000^{-1}}\right)^{1/7} \left(\frac{x_M}{300}\right)^{-3/7} \left(\frac{\alpha}{0.3}\right)^{3/14} \left(\frac{1-\beta}{0.5}\right)^{-1/14} \\ &\times \left(\frac{c_1}{0.5}\right)^{3/14} \left(\frac{c_3}{0.3}\right)^{-1/14} \left(\frac{r_{\rm min}}{3}\right)^{3/28} m^{1/14}\, \dot{m}^{-1/14} \;\; {\rm K}, \end{aligned} \tag{40}$$

where $A_c^{1/7}$ varies from 0.95 to 1.4, and we have scaled x_M appropriately for low $\dot{m}$ (cf. Fig. 2). Fig. 2 shows the temperature increasing faster with $\dot{m}$ than indicated above. This is mainly due to the sensitivity of the temperature on x_M, which decreases since the synchrotron emission decreases as $\dot{m}^2$. However, comparing the four panels in Fig. 2, shows that the temperature is fairly insensitive to the mass of the central black hole.

<u>$\alpha_c < 1$.</u>

In this regime we find simple recursive formulae that can be used to determine T_e analytically. For $\alpha_c < 1$, both synchrotron and bremsstrahlung cooling is negligible, and the total cooling, Q^- is given by eq.(35)

$$\begin{aligned} Q^{-} \simeq P_{\rm Compton} &= \frac{\nu_p \, L_{\nu_p}}{1 - \alpha_c} \left[\left(\frac{6.2 \times 10^7 \, (T_e/10^9)}{(\nu_p/10^{12})} \right)^{1-\alpha_c} - 1 \right], \\ &\equiv \frac{\nu_p \, L_{\nu_p}}{1 - \alpha_c} \left(C_F^{1-\alpha_c} - 1 \right), \end{aligned} \tag{41}$$

where the Compton factor C_F has been defined for convenience. When $\alpha_c < 1$, $\dot{m} \gtrsim 10^{-3}\alpha$ and from eq.(15) $\delta\, Q^{+}$ is negligible compared with Q^{ie}. Therefore $Q^{\rm e+} \simeq Q^{ie}$. Instead of equating Q^{ie} to $P_{\rm Compton}$, and solving for the temperature, a good approximation to the temperature can be obtained by rewriting eq. (34) as a quadratic,

$$1 + 4\theta_e + 16\theta_e^2 = \tau_{es}^{-1/\alpha_c}, \tag{42}$$

which gives,

$$\left(\frac{T_e}{10^9}\right) = 0.744 \left[\left(4\, \tau_{es}^{-1/\alpha_c} - 3 \right)^{1/2} - 1 \right]. \tag{43}$$

Since $0.5 \leq \alpha_c \leq 1.0$ for all cases of interest, we can get an idea for the range of temperatures possible for a given $\dot{m}$ by setting $\alpha_c = 0.5$, and $\alpha_c = 1.0$ (lower values of α_c would require very high $\dot{m}$, and this is where the advection solutions are no longer valid). This gives

$$2.15 \times 10^8 \, \dot{m}^{-1/2} \lesssim T_e \lesssim 3.12 \times 10^7 \, \dot{m}^{-1}. \tag{44}$$

For high $\dot{m} \sim 10^{-2}$ systems in this regime, eq.(44) indicates that the range of temperatures possible is confined to $2.15 \times 10^9 \leq T_e \leq 3.12 \times 10^9$, whether the systems are $1 M_\odot$ or $10^9 M_\odot$ black holes (cf. Fig. 2). However as $\dot{m}$ decreases, while $\alpha_c < 1$, the temperature range possible increases (eg. for $\dot{m} \sim 10^{-2.5}$, $3.8 \times 10^9 \leq T_e \leq 9.8 \times 10^9$), and a more accurate evaluation of α_c is necessary.

We can determine, to a first approximation, the temperature in these systems by setting $\alpha_c \sim 0.75$ in eq.(43). From this estimate, a more accurate determination of α_c can be obtained by equating Q^{ie} to eq.(41), and rewriting to give

$$1 - \alpha_c = \log \left[\frac{Q^{ie}}{\nu_p \, L_{\nu_p}} \, (1 - \alpha_c) + 1 \right] \Big/ \log(C_F). \tag{45}$$

Since logarithms are slowly varying functions, α_c in the logarithm can be set to ~ 0.75, as before, to obtain

$$1 - \alpha_c \simeq \log \left(\frac{Q^{ie}}{4 \, \nu_p \, L_{\nu_p}} - 1 \right) \Big/ \log(C_F). \tag{46}$$

where $1 - \alpha_c$ is the slope of the spectrum on a $\nu \, L_\nu$ plot,

$$\begin{aligned} \frac{Q^{ie}}{\nu_p \, L_{\nu_p}} &= 3.57 \times 10^2 \left(\frac{x_M}{1000} \right)^{-3} \left(\frac{\alpha}{0.3} \right)^{-1/2} \left(\frac{\beta}{0.5} \right) \left(\frac{1-\beta}{0.5} \right)^{-3/2} \left(\frac{c_1}{0.5} \right)^{-1/2} \\ &\times \left(\frac{c_3}{0.3} \right)^{-1/2} \left(\frac{r_{\rm min}}{3} \right)^{3/4} \left(\frac{T_e}{10^9} \right)^{-7} g(\theta_e) \, m^{1/2} \, \dot{m}^{1/2}, \end{aligned} \tag{47}$$

and

$$\begin{aligned} C_F &= 1.46 \times 10^3 \left(\frac{x_M}{1000} \right)^{-1} \left(\frac{\alpha}{0.3} \right)^{1/2} \left(\frac{1-\beta}{0.5} \right)^{-1/2} \left(\frac{c_1}{0.5} \right)^{1/2} \\ &\times \left(\frac{c_3}{0.3} \right)^{-1/2} \left(\frac{r_{\rm min}}{3} \right)^{5/4} \left(\frac{T_e}{10^9} \right)^{-1} m^{1/2} \, \dot{m}^{-1/2}. \end{aligned} \tag{48}$$

Solving for α_c then gives a better approximation for the temperature from eq.(43). This process can be iterated for accurate determination of both T_e and α_c, but we find that fairly accurate results are obtained without any iterations.

5.2. Total Luminosity.

For a given accretion rate $\dot{M}$, and matter to energy conversion of $\eta_{\rm eff} = 0.1$, standard accretion disks predict a total luminosity of $L_{\rm disk} \simeq \eta_{\rm eff}\, \dot{M}\, c^2$. Advection dominated accretion produces a lower luminosity because most of the viscously dissipated energy is advected inwards with the flow and deposited into the black hole instead of being radiated. The total luminosity from these disks is equal to the total energy being emitted by the various cooling processes, $L_{\rm ADAF} = Q^-$. However since $Q^{\rm e+} = Q^-$, detailed knowledge of the cooling processes is not required here, and the total luminosity is simply $L_{\rm ADAF} = Q^{\rm e+}$.

Depending on the value of $\dot{m}$, the total heating of the electrons is either dominated by Q^{ie} or by $\delta\, Q^+$. The luminosities in both these regions are determined by setting $L_{\rm adv} = \max(Q^{ie}, \delta\, Q^+)$. For $\dot{m} > 10^{-3}\, \alpha^2$ (cf. eq. 15), Q^{ie} dominates, and the total luminosity is given by

$$
\begin{aligned}
L_{\rm ADAF} &\simeq 1.2 \times 10^{38}\, g(\theta_e)\, c_1^{-2}\, c_3\, \beta\, r_{\rm min}^{-1}\, \alpha^{-2}\, m\, \dot{m}^2, \\
&\simeq \eta_{\rm eff} \dot{M}\, c^2 \left[0.20\, \left(\frac{\dot{m}}{\alpha^2}\right)\, g(\theta_e)\, \left(\frac{\beta}{0.5}\right) \left(\frac{c_1}{0.5}\right)^{-2} \left(\frac{c_3}{0.3}\right) \left(\frac{r_{\rm min}}{3}\right)^{-1} \right] \ \text{ergs s}^{-1},
\end{aligned}
\tag{49}
$$

where c is the speed of light. This also gives the luminosity for the case $\delta = 0$. For $\dot{m} \lesssim 10^{-3}\, \alpha^2$, $\delta\, Q^+$ dominates the electron heating and the total luminosity can be written as

$$
L_{\rm ADAF} \simeq \eta_{\rm eff}\, \dot{M}\, c^2 \left[2.0 \times 10^{-4} \left(\frac{\delta}{2000^{-1}}\right) \left(\frac{1-\beta}{0.5}\right) \left(\frac{c_3}{0.3}\right) \left(\frac{r_{\rm min}}{3}\right)^{-1} \left(\frac{f}{1.0}\right)^{-1} \right] \ \text{ergs s}^{-1}.
\tag{50}
$$

The factor in the square brackets is the factor by which the efficiency is reduced relative to the usual 10% from standard thin accretion disks. At high accretion rates, the luminosity decrease linearly with $\dot{m}$, but there is no additional $\dot{m}$ dependence at low accretion rates since the ion–electron transfer rate becomes very inefficient, and the cooling processes have to compensate only for a fraction of the viscous heating generated. Using $L_{\rm ADAF} = Q^{e+}$, and the numerical method in §5.1.1., Fig. 4 shows plots of $L_{\rm ADAF}/L_{\rm Edd}$ as a function of $\dot{m}$ for various values of α. Disks with high values of α are more sub–Eddington in their luminosities that disks with low α. At low $\dot{m}$ the luminosities are independent of α (cf. eq. 50). Although Fig. 4 is calculated for $m = 10^9$, it can be used for any value of m, since the ratio $L_{\rm ADAF}/L_{\rm Edd}$ is independent of m, and the equilibrium temperatures are fairly insensitive to the exact value of m.

5.3. Determining $\dot{m}_{\rm crit}$.

In advection flows where $\dot{m} \ll 1$, Narayan & Yi (1995b) have shown that $f \simeq 1$. However as $\dot{m}$ increases, the Coulomb interactions between the ions and electrons

become more efficient, and more of the viscously generated energy is transferred from the ions to the electrons. This decreases the amount of energy that can be advected inwards with the flow, and the value of f therefore also decreases. As $\dot{m}$ is increased further, the flow radiates the generated heat more efficiently, becomes less advection dominated, and becomes optically thick. Narayan & Yi (1995b) have shown that for $\dot{m}$ greater than a critical value, $\dot{m}_{\rm crit}$, the energy equations (cf. 8) have no solution, and the advection dominated solution ceases to exist. Here, we determine what $\dot{m}_{\rm crit}$ is, for a given set of parameters m, α, β.

To determine the critical accretion rate, the energy equation becomes $Q^{+}(1-f) = Q^{-} \simeq Q^{ie}$, since $Q^{ie} \gg \delta Q^{+}$ in this regime ($\dot{m} \gg 10^{-3}\alpha^2$). Dividing eq.(9) by eq.(13), and rewriting in terms of $\dot{m}$ gives

$$\dot{m} = 7.8\,\frac{(1-f)}{f}\,\frac{(1-\beta)}{\beta}\,\alpha^2\,c_1^2\,\frac{1}{g(\theta_e)}. \tag{51}$$

When $\dot{m} \sim \dot{m}_{\rm crit}$, we expect $f \sim 0.5$, which requires about half the generated energy to be radiated away, which is a reasonable assumption. Also, for very high $\dot{m} \sim 10^{-1.7}$, eq.(44) shows that $T_e \sim 1.5 \times 10^9$ which gives $g(\theta_e) \sim 7$. Setting $\beta = 0.5$, $c_1 \simeq 0.5$, gives

$$\dot{m}_{\rm crit} \simeq 0.28\,\alpha^2. \tag{52}$$

The critical accretion rate, in scaled units, is therefore independent of the mass of the accreting object, but depends quite strongly on α. This suggests a large value of $\alpha \sim 1$ since a low value of $\alpha \sim 0.01$ gives a very small $\dot{m}_{\rm crit}$, which is not luminous enough to explain even moderate luminosities. Advection models that have had success in explaining black hole candidates (eg. Lasota et al. 1996; Narayan et al. 1995) use $\alpha \sim 0.1 - 0.3$, and, as suggested by Narayan (1996), could be as high as ~ 1 to explain low luminosity AGNs.

6. Do Elliptical Galaxies Host Dead Quasars?

In this section we use the results above and apply them to a specific problem which was first suggested by Fabian & Canizares (1988). We give a brief introduction to the problem, derive the results of Fabian & Canizares (1988), and then, as suggested by Fabian & Rees (1995) show how advection–dominated accretion flows resolve this problem.

6.1. Outline.

Most nearby bright elliptical galaxies are believed to host 'dead' or inactive quasars (Soltan 1982; Fabian & Canizares 1988; Fabian & Rees 1995). From energetic arguments or from the properties of broad line emitting regions, the masses of quasars are found to be between $10^8 - 10^9 M_\odot$ (Wandel & Mushotzky 1986). We should therefore expect black hole masses of this size at the cores of bright elliptical galaxies, and should be able to detect accretion of the ambient gas onto the central black hole.

From X-ray profiles of elliptical galaxies, we can determine the density and temperature of the gas within the central kilo–parsec region. Since elliptical galaxies are thermally supported, and are most likely to spherically accrete, we can use the classical Bondi formula to obtain what is essentially a lower limit to the luminosity produced by a black hole of a given mass. Fabian & Canizares (1988) have looked at six bright nearby ellipticals and, from the observed X-ray luminosity of the gas, have determined upper limits for the black hole masses in these galaxies to be $< 3 \times 10^7 M_\odot$. This is in conflict with the expected masses, in these galaxies, as determined by Soltan (1982), together with the independent estimates of quasar masses as determined by Wandel & Mushotzky (1986). One of the conclusions is to reject the black hole hypothesis for quasars, since requiring higher mass black holes, would lead to a higher luminosity in the X-rays, which is not observed. To reconcile these differences, Fabian & Rees (1996) have recently suggested that the massive black holes at the centers of these galaxies might be undergoing advection dominated accretion which would help reconcile these differences.

6.2. Standard Accretion.

In this section we show how Fabian & Canizares (1988) use standard Bondi accretion to deduce severe upper limits to the masses of the black holes at the centers of bright elliptical galaxies.

A lower limit on the accretion luminosity is obtained by assuming that the gas accretes spherically onto the central black hole by Bondi accretion. Following Fabian & Canizares (1988), the accretion radius, the radius at which the influence of gravity by the central black hole dominates the dynamics of the gas, is $R_{acc} = \alpha_b \, G \, M/c_s^2 = 4.32 \; \alpha_b \, M_8 \, T_7^{-1}$ pc, where $c_s \simeq 10^4 \; T^{1/2}$ cm s^{-1}, and α_b is a factor including the ratio of specific heats (see Bondi 1952). $\alpha_b > 0.5$ and is probably ~ 1. The Bondi accretion rate is given by $\dot{M} = 1.86 \times 10^{-4} \; \alpha_b^2 \, P_6 \, T_7^{-5/2} \, M_8^2 \;\; M_\odot$ yr^{-1}, where we have written $P = n_e \, T = 10^6 P_6$ cm^{-3} K, to keep the notation of Fabian & Canizares (1988). This gives a luminosity assuming a 10% matter to energy conversion, of

$$L_b = 1.06 \times 10^{42} \; \alpha_b^2 \, P_6 \, T_7^{-5/2} \, M_8^2 \;\; \text{ergs s}^{-1}. \tag{53}$$

From eq.(53), if $P_6 = T_7 = 1$, black hole masses of $10^8 - 10^9 M_\odot$ should be detectable.

P_6 and T_7 can be determined by looking at the radial X-ray profiles of elliptical galaxies. Canizares et al. (1987) find the mean temperatures of the gas to be $\sim 0.5 - 4 \times 10^7$ K, and determine the central number density by calculating the volume emissivity of the X-ray gas, $\epsilon = 4\pi\, n_e(0)^2\, a_X^2\, [\ln(2R_X/a_X) - 1]$ cm^{-3}, where a_X is the core radius, and R_X is the maximum radial extent of the gas which is chosen to be $50\, a_X$. (This choice is consistent with the radial profiles in Trinchieri et al. 1986.) Using the cooling function $\Lambda(T) = 10^{-19}\, T^{-1/2}$ ergs cm^3 s^{-1}, the central density is

$$\begin{aligned} n_e(0) &= \left(\frac{L_X}{\Lambda(T)\, 4\pi\, a_X^3\, 3.61}\right)^{1/2} \quad \mathrm{cm}^{-3} \\ &= 4.88 \times 10^{-2} \left(\frac{L_X}{10^{41}\,\mathrm{ergs\ s^{-1}}}\right)^{1/2} \left(\frac{a_X}{1\,\mathrm{kpc}}\right)^{-3/2} T_7^{1/4} \quad \mathrm{cm}^{-3} \end{aligned} \tag{54}$$

We assume that the central density $n_e(0)$ evaluated continues on to the central black hole, i.e. there is no central cavity in these galaxies. Using $P = n_e\, T$ in eq.(53) the expected X-ray luminosity from accretion in terms of the total observed X-ray luminosity from the gas, is given by

$$L_b = 5.17 \times 10^{41}\ \alpha_b^2\, M_8^2\, T_7^{1/4}\, (a^3\, T_7^3)^{-1/2} \left(\frac{L_X}{10^{41}}\right)^{1/2} \quad \mathrm{ergs\ s^{-1}}, \tag{55}$$

where $a = (a_X/1$ kpc). This corresponds to an accretion rate in Eddington units of

$$\dot{m} = 4.16 \times 10^{-5}\ \ \alpha_b^2\, M_8\ T_7^{1/4}\, (a^3\, T_7^3)^{-1/2} \left(\frac{L_X}{10^{41}}\right)^{1/2}. \tag{56}$$

Rewriting eq.(55) to resemble Fabian & Canizares (1988), and setting $\alpha_b = 0.5$, we have

$$\frac{L_b}{L_X} = 1.3\ M_8^2 \left[\left(\frac{L_X}{10^{41}}\right) a^3\, T_7^3\right]^{-1/2} T_7^{1/4}. \tag{57}$$

The quantity L_b/L_X is a measured quantity which is obtained by using the X-ray profiles of the elliptical galaxies, and taking the ratio of the X-ray emission from the central arcsecond region to the total X-ray gas emission from the whole galaxy. Table 2 shows the parameters used for three of the six galaxies analyzed by Fabian & Canizares (1988). These galaxies were chosen since they have good Einstein HRI data (Trinchieri et al. 1986). The core X-ray luminosities were estimated from the surface brightness profiles given in Trinchieri et al. (1986), taking into account the resolution of the detector. The best fits for the core radius a_X and temperature T_7 was also taken from Trinchieri et al. (1986). Using eq.(57) and the best fit parameters, Table 2 shows the upper limits for black hole masses using Bondi accretion. These limits are much too low to be consistent with expected masses.

6.3. Advection–Dominated Accretion.

We now show, as suggested by Fabian & Rees (1995), that advection–dominated accretion resolves this problem. Using the scaling laws derived here, we can estimate upper limits to the black hole masses. From eq. (56), we find that for black hole masses of $\sim 10^{8-10} M_\odot$, $\dot{m} \sim 10^{-3} - 10^{-5}$ and we are in the regime where the total luminosity is determined by eq. (49). We also expect $\alpha_c > 1$ for these systems, and therefore can set $g(\theta_e) \sim 1$ in eq.(49) (cf. eq. 40). Setting $c_1 = 0.5$, $c_3 = 0.3$, $\beta = 0.5$, $r_{\rm min} = 3$, eq.(49) gives

$$L_{\rm ADAF} \simeq \eta_{\rm eff}\, 0.20\, \dot{M} \left(\frac{\dot{m}}{\alpha^2}\right) c^2, \quad {\rm ergs\ s^{-1}}, \tag{58}$$

This is the total luminosity which is emitted over eight orders in magnitude of frequency. Assuming that a fraction, η_X, of this energy is radiated into the 0.2 – 4.0 keV band in the X-rays (Trinchieri et al. 1986), the luminosity in this band from the advection dominated disk is simply $L_{b_{\rm ADAF}} = \eta_X\, L_{\rm ADAF}$. Multiplying eq.(55) by $0.20\, \eta_X\, \dot{m}/\alpha^2$ gives

$$\frac{L_{b_{\rm ADAF}}}{L_X} = 4.3 \times 10^{-5}\, \eta_X \left(\frac{\alpha_b^4}{\alpha^2}\right) M_8^3\, (a^3 T_7^3)^{-1}\, T_7^{-1/2}. \tag{59}$$

Taking $\alpha_b = 0.5$, as in eq.(57), and $\alpha = 0.3$, a typical value for advection models, eq.(59) becomes

$$M_8 \simeq 32.2\ \eta_X^{-1/3} \left(\frac{\alpha}{0.3}\right)^{2/3} \left(\frac{L_{b_{\rm ADAF}}}{L_X}\right)^{1/3} a\, T_7^{7/6}. \tag{60}$$

The last column in Table 2 shows upper bounds for the masses of the black holes in these galaxies using $\eta_X = 1$, (a very conservative estimate) from the advection models. The upper limits shown are much higher than those of Fabian & Canizares (1988). A maximum value of η_X is obtained by arbitrarily setting $\alpha_c = 1$. This gives a flat spectrum on a νL_ν plot, and since the total emission occurs over eight orders in magnitude of frequency, and the observations are made only in the 0.2 – 4.0 keV band, ~ 1 order in magnitude, $\eta_X \lesssim 1/8 \simeq 0.13$. This corresponds to increasing the upper limits in Table 2 by a factor of ~ 2. Furthermore since $\alpha_c > 1$ in these systems, η_X would probably be significantly lower, and this would raise the upper limits even more. Fig. 5 shows the upper limits of the core X-ray emission, from the galaxies in Table 2, in the 0.2 – 4 keV band, and shows the spectrum from an advection–dominated disk for $m = (0.5, 5, 10, 30) \times 10^8$, with the corresponding $\dot{m}$ given by eq.(56), and $\alpha = 0.3$, $\beta = 0.5$. Clearly, the value of $\eta_X \lesssim 0.13$, and easily allows for black hole masses $\lesssim 10^{10} M_\odot$ at the centers of bright ellipticals, consistent with the idea that bright elliptical galaxies do host dead quasars.

7. Discussion & Conclusion.

The advection models are very robust in that they have very characteristic spectra: a $\nu^{1/3}$ slope in the radio regime, a sub-mm to X-ray Compton spectrum,

and a bremsstrahlung spectrum. If we assume that a system is going through advection–dominated accretion, as in the case of the elliptical galaxies above, we can make predictions of what the spectrum should look like. With α, β fixed, and $\dot{m}$ given by eq.(56), the only free parameter that can be varied is the mass. Once this is fixed, the entire spectrum is completely determined. The radio spectrum in these elliptical galaxies should follow a $\sim \nu^{1/3}$ slope, which extends up to a peak frequency, ν_p. Radio observations of these galaxies would therefore determine their core masses, and would lead to testable predictions for the X-ray fluxes. Note that the inclusion of a thin disk might change the optical and ultra–violet region of the spectrum, but would not affect the strong correlation between the radio and X-ray fluxes (eg. Lasota et al. 1996). Observations in the radio of these elliptical galaxies have been done (Wrobel 1991). Although Wrobel (1991) observers weak jets at the cores of these elliptical galaxies, upper limits to the unresolved compact core emission has been obtained. These upper bounds are shown in Fig. 5. We see that the radio bounds are quite consistent with black hole masses $m \gtrsim 10^9$. The masses of NGC 4636, 4649, and 4472, in this simple description are constrained to be less than 10^9, 2×10^9, and 3×10^9 $M_\odot$ respectively. This is a remarkable testable feature of the advection models: to explain the entire spectra of these systems using few free parameters.

Interestingly, Slee et al. (1994) have observed radio spectra in other bright elliptical galaxies, and obtain an average radio spectral index of 1/3. If this is emission from a compact core, it is generally accepted to be from a non–thermal source of electrons (eg. Duschl & Lesch 1994). However, if these low luminosity systems are advection–dominated flows, then the thermal self–absorbed synchrotron radiation from these models naturally give rise to the characteristic 1/3 spectrum produced by optically thin non–thermal synchrotron emission.

Another interesting application of these models is to explain low luminosity Active Galactic Nuclei (AGNs, Narayan 1996). We again use the strong correlation between the radio and X-ray fluxes. The luminosity of quasars in the X-rays are $\gtrsim 10^{44}$ ergs s^{-1}, and their accretion rates are $> \dot{m}_{\rm crit}$. However, as the accreting rate decreases and falls below $\dot{m}_{\rm crit}$ the accreting gas might prefer to follow an advection flow (Narayan & Yi 1995b). Since $\dot{m}_{\rm crit}$ is independent of m, all AGNs making this transition would have very hard X-ray spectra with spectral indices ~ 0.7, since $\alpha_c < 1$. Since the temperature of all systems near $\dot{m}_{\rm crit}$ are well determined (cf. Fig. 2 and §5.1.2.), we can get a good estimate of $\dot{m}$ using eq.(34). This could then be combined with the X-ray luminosity to give an estimate of the mass of the central object. With the mass, accretion rate and temperature of these systems, the advection–dominated models can be used to make predictions of the radio spectrum from these sources. Recently Ho (1996) has obtained observations of nearby galaxies which show AGN-like spectral lines, are underluminous, and have steep X-ray spectra. Observations in the radio of these galaxies would not only serve as a test for the advection models, but would also independently determine the masses of the central objects.

We have shown that the general properties of optically thin advection dominated flows can be easily understood through simple scaling laws. The spectra that these models produce can be reproduced fairly well from a basic knowledge of the three electron cooling processes. For high $\dot{m}$, the Compton power is the dominant source of cooling which gives a very hard X-ray spectrum. In the opposite limit, for low $\dot{m}$, synchrotron cooling dominates the cooling, and most of the energy is emitted in the radio. The bremsstrahlung power is negligible, but depending on the amount of Compton power, can dominate the X-ray emission.

These results have been applied to determine, as suggested by Fabian & Canizares (1988), and more recently by Fabian & Rees (1996), whether dead quasars are at the centers of elliptical galaxies. We have found that if these are advection–dominated systems, which is most likely due to the low accretion rates, then the upper limits are much higher $M \lesssim 5 \times 10^9 M_\odot$ than that determined by Fabian & Canizares (1988) $M \lesssim 3 \times 10^7 M_\odot$. Therefore we are allowed to have black hole masses of $M \lesssim 10^{10} M_\odot$ at the centers of bright ellipticals as required by independent arguments.

The advection models are constantly tested by observations. Since there are few free parameters in the model, and the predicted spectrum ranges over all observable frequencies, failure to comply with any observation would pose serious problems. All the observations on putative $1 M_\odot$ to $10^9 M_\odot$ advection dominated black hole systems have so far agreed quite well with predictions.

Acknowledgments: The author thanks Ramesh Narayan for many useful discussions and comments, and the referee A. C. Fabian for helpful suggestions. This work was supported by NSF grant AST 9423209.

A. Analytic Approximation to q^{ie}.

The energy transfer rate from the ions to electrons via Coulomb collisions is given by Stepney & Guilbert (1983)

$$q^{ie} = 5.61 \times 10^{-32} \frac{n_e^2 (T_i - T_e)}{K_2(1/\theta_e)\, K_2(1/\theta_i)} \times \left[\frac{2(\theta_e+\theta_i)^2+1}{(\theta_e+\theta_i)} K_1\left(\frac{\theta_e+\theta_i}{\theta_e\,\theta_i}\right) + 2K_0\left(\frac{\theta_e+\theta_i}{\theta_e\,\theta_i}\right)\right] \text{ ergs cm}^{-3}\text{ s}^{-1}. \tag{A1}$$

The following identities hold for the temperature range of interest,

$$10^9 < T_i < 10^{12}, \quad 10^{-4} < \theta_i < 10^{-1}, \quad 10 < \theta_i^{-1} < 10^4, \tag{A2}$$

and

$$10^9 < T_e < 10^{10}, \quad 0.17 < \theta_e < 1.7, \quad .6 < \theta_e^{-1} < 6. \tag{A3}$$

The arguments of the modified Bessel functions K_0 and K_1 are large for these values of θ_e and θ_i which enable the use of the approximation (Abramowitz & Stegun 1964, 9.7.2)

$$K_n(x) \simeq \sqrt{\frac{\pi}{2\,x}}\, e^{-x} \left(1 + \frac{4n^2-1}{8\,x} + \ldots\right). \tag{A4}$$

Since $\theta_i \ll 1$, terms of order $O(\theta_i/\theta_e)$ can be neglected. This gives

$$K_0\left(\frac{\theta_e+\theta_i}{\theta_e\,\theta_i}\right) \simeq \sqrt{\frac{\pi}{2}} \left(\frac{\theta_e\,\theta_i}{\theta_e+\theta_i}\right)^{1/2} e^{-1/\theta_i}\, e^{-1/\theta_e} \tag{A5}$$

$$K_1\left(\frac{\theta_e+\theta_i}{\theta_e\,\theta_i}\right) \simeq \sqrt{\frac{\pi}{2}} \left(\frac{\theta_e\,\theta_i}{\theta_e+\theta_i}\right)^{1/2} e^{-1/\theta_i}\, e^{-1/\theta_e} \tag{A6}$$

$$K_2\left(\frac{1}{\theta_i}\right) \simeq \sqrt{\frac{\pi}{2}}\, \theta_i^{1/2}\, e^{-1/\theta_i}. \tag{A7}$$

Eq.(A1) then becomes

$$q^{ie} \simeq 5.61 \times 10^{-32} \frac{n_e\, n_i\, (T_i - T_e)}{K_2(1/\theta_e)} \times \left(\frac{\theta_e\,\theta_i}{\theta_i(\theta_e+\theta_i)}\right)^{1/2} \left[\frac{2(\theta_e+\theta_i)^2+1+2(\theta_e+\theta_i)}{(\theta_e+\theta_i)}\right] e^{-1/\theta_e} \text{ ergs cm}^{-3}\text{ s}^{-1}, \tag{A8}$$

which simplifies to

$$q^{ie} \simeq 5.61 \times 10^{-32}\, n_e\, n_i\, (T_i - T_e)\, g(\theta_e) \text{ ergs cm}^{-3}\text{ s}^{-1}. \tag{A9}$$

where

$$g(\theta_e) \equiv \frac{1}{K_2(1/\theta_e)} \left(2 + 2\theta_e + \frac{1}{\theta_e}\right) e^{-1/\theta_e}. \tag{A10}$$

Values of $g(\theta_e)$ are given in Table 1.

B. Determining x_M

From eq.(20) we have

$$\exp\left(1.8899\, x_M^{1/3}\right) = 2.49 \times 10^{-10}\, \frac{4\pi\, n_e\, R}{B}\, \frac{1}{\theta_e^3\, K_2(1/\theta_e)} \left(\frac{1}{x_M^{7/6}} + \frac{0.40}{x_M^{17/12}} + \frac{0.5316}{x_M^{5/3}}\right). \tag{B11}$$

Since most systems of interest are highly self-absorbed, x_M will be large, and therefore fairly independent of r. [2] In this case, we can set $r = 3$ in eq.(B11), and neglect the last two terms in the parentheses (this can be checked for self consistency). Substituting for n_e, R, and B from eqs.(5) in eq.(B11), and taking logarithms on both sides, gives

$$\begin{aligned} y + 1.852 \ln y &\simeq 10.36 + 0.26 \ln(m\, \dot{m}) - 0.26 \ln\left[\theta_e^3\, K_2\,(1/\theta_e)\right] \\ &- 0.26 \ln\left[\left(\frac{\alpha}{0.3}\right)\left(\frac{c_1}{0.5}\right)\left(\frac{c_3}{0.3}\right)\left(\frac{1-\beta}{0.5}\right)\right]. \end{aligned} \tag{B12}$$

where

$$y = x_M^{1/3}.$$

This equation can be solved numerically, and Table 1 shows the values of $\theta_e^3\, K_2\,(1/\theta_e)$ for the temperature range of interest. Fig. 2 shows plots of x_M as a function of $\dot{m}$ for different values of black hole mass m, where the value of x_M is determined after solving for the equilibrium temperature in the flows (cf. §5.1.1.). Since x_M is weakly dependent on m, α, β, but depends mainly on $\dot{m}$, we have a useful formula for the dependence of x_M on $\dot{m}$

$$\log x_M = 3.6 + \frac{1}{4} \log \dot{m}, \tag{B13}$$

which can be used for different values of m, α and β to a good approximation.

C. Formulae for $\delta = 0$.

In this appendix we give formulae for $\delta = 0$. In §5.1.2. we obtained an equation for the temperature for $\alpha_c > 1$ where we neglected Q^{ie} compared with $\delta\, Q^+$. If $\delta = 0$ or $\dot{m} \geq 10^{-4}$ the temperature has to be determined by setting

$$\begin{aligned} Q^{ie} = Q^- &\simeq \left(0.71 + \frac{1}{\alpha_c - 1}\right) \nu_p\, L_{\nu_p} \\ &\simeq A_c\, \nu_p\, L_{\nu_p}, \end{aligned} \tag{C14}$$

[2]Numerical calculations have shown that $x_M \sim r^{1/15}$, for $r \lesssim 10^3$.

where the first term is due to synchrotron cooling and the second is due to Compton cooling. Using eq. (13) and rewriting, gives

$$\frac{T_e^7}{g(\theta_e)} \simeq \frac{1.2\times 10^{74}}{A_c}\, x_M^{-3}\, \alpha^{-1/2}\, \beta\, (1-\beta)^{-3/2}\, c_1^{-1/2}\, c_3^{-1/2}\, m^{1/2}\, \dot{m}^{1/2}\, r_{\rm min}^{3/4}. \tag{C15}$$

To simplify further, $g(\theta_e)$ can be approximated to

$$g(\theta_e) \simeq 1.91\times 10^{11}\, T_e^{-1.1464}, \tag{C16}$$

which is valid for 10^9 K $\leq T_e \leq 3\times 10^{10}$ K, and has a maximum error of 20% at $T_e \sim 10^9$. [3] Using this approximation and canonical values of the constants gives

$$\begin{aligned} T_e \;\simeq\;& \frac{2.7\times 10^9}{A_c^{3/25}} \left(\frac{x_M}{1000}\right)^{-2/5} \left(\frac{\alpha}{0.3}\right)^{-3/50} \left(\frac{\beta}{0.5}\right)^{3/25} \left(\frac{1-\beta}{0.5}\right)^{-1/5} \left(\frac{c_1}{0.5}\right)^{-3/50} \\ \times\;& \left(\frac{c_3}{0.3}\right)^{-3/50} \left(\frac{r_{\rm min}}{3}\right)^{1/10} m^{3/50}\, \dot{m}^{3/50}\ \ {\rm K}, \end{aligned}$$

where $0.96 \leq A_c^{3/25} \leq 1.3$, and we have approximated the exponents to the nearest fraction.

[3] The error made in this approximation is reduced when taking the $\sim 1/7^{th}$ power to determine T_e.

Table 1: θ_e and $K_2(1/\theta_e)$.

T_9	θ_e	$g(\theta_e)$	$\theta_e^3\,K_2(1/\theta_e)$
1.00	0.1686	12.003	8.783e–06
1.50	0.2530	6.7292	2.982e–04
2.00	0.3373	4.5134	2.472e–03
2.50	0.4216	3.3386	1.092e–02
3.00	0.5059	2.6261	3.408e–02
3.50	0.5902	2.1540	8.550e–02
4.00	0.6746	1.8209	1.849e–01
4.50	0.7589	1.5746	3.593e–01
5.00	0.8432	1.3859	6.438e–01
5.50	0.9275	1.2369	1.083e+00
6.00	1.0118	1.1166	1.731e+00
6.50	1.0961	1.0175	2.654e+00
7.00	1.1805	0.9345	3.930e+00
7.50	1.2648	0.8640	5.650e+00
8.00	1.3491	0.8035	7.922e+00
8.50	1.4334	0.7509	1.086e+01
9.00	1.5177	0.7048	1.462e+01
9.50	1.6021	0.6641	1.933e+01
10.00	1.6864	0.6278	2.519e+01

Table 2: Galaxies analyzed from Fabian & Canizares (1988). Distances are taken from Trinchieri et al. (1986).

Galaxy NGC	Distance Mpc	M_B	a_X kpc	T_7	$\log(L_X)$	L_b/L_X	$10^8\,M_\odot$ (FC)	$10^8\,M_\odot$ (Advection)
4472	20	-22.8	0.48	1.4	41.71	0.025	0.14	6.7
4649	20	-22.2	0.96	1.4	41.40	0.047	0.29	24.1
4636	16.4	-21.6	1.18	1.2	41.64	0.030	0.27	14.6

References

Abramowitz, M., & Stegun, A. I., 1965, Handbook of Mathematical Functions (National Bureau of Standards, Washington, D. C.)

Abramowicz, M., Chen, X., Kato, S., Lasota, J. P, & Regev, O., 1995, ApJ, 438, L37

Abramowicz, M., Czerny, B., Lasota, J. P, & Szuszkiewicz, E., 1988, ApJ, 332, 646

Bondi, H., 1952, MNRAS, 112, 195-204

Canizares, C. R., Fabbiano, G., & Trinchieri, G., 1987, ApJ, 312, 503-513

Dermer, C. D., Liang, E. P., & Canfield, E., 1991, ApJ, 369, 410

Duschl, W., & Lesch, H., 1994, A& A, 286, 431-436

Esin, A., in preparation

Fabian, A. C., & Canizares, C. R., 1988, Nature, 333, 829-831

Fabian, A. C., & Rees, M. J., 1995, MNRAS, 277, L55-L58

Frank, J., King, A., & Raine, D., 1992, Accretion Power in Astrophysics (Cambridge: Cambridge Univ. Press)

Haswell, A. C., Robinson, L. E., Horne, K., Stiening, F. R., Abbott, M. C. T., 1993, ApJ, 411, 802-812

Ho, C. L., 1996, in The Physics of LINERS in View of Recent Observations, eds. Eracleous, M., Koratkar, P. A., Ho, C. L., & Leitherer, C., (San Francisco: ASP)

Lasota, J. P., Abramowicz, M. A., Chen, X., Krolik, J., Narayan, R., & Yi, I. 1996, ApJ, in press

Mahadevan, R., Narayan, R., & Yi., I., 1996, ApJ, 465, 327-337

Matsumoto, R., Kato, S., & Fukue, J., 1985, in Proc. Symposium on Theoretical Aspects of Structure, Activity, and Evolution of Galaxies: III, ed. S. Aoki, M. Iye, and Y. Yoshii, (Tokyo: Tokyo Astron. Obs.), 102

Narayan, R., 1996, ApJ, 462, 136

Narayan, R., McClintock, J. E., & Yi, I., 1996, ApJ, 457, 821-833

Narayan, R., & Yi, I., 1994, ApJ, 428, L13

Narayan, R., & Yi, I., 1995a, ApJ, 444, 231

Narayan, R., & Yi, I., 1995b, ApJ, 452, 710-735

Narayan, R., Yi, I., & Mahadevan, R., 1995, Nature, 374, 623-625

Narayan, R., Yi, I., & Mahadevan, R., 1996, A&A, in press

Rees, M. J., Begelman, M. C., Blandford, R. D., & Phinney, E. S., 1982, Nature, 295, 17

Rybicki, G., & Lightman, A., 1979, Radiative Processes in Astrophysics (New York: John Wiley & Sons, Inc.)

Shapiro, S. L., Lightman, A. P., & Eardley, D. M. 1976, ApJ, 204, 187

Slee, O. B., Sadler, E. M., Reynolds, J. E., & Ekers, 1994, MNRAS, 269 , 928-946

Stepney, S., & Guilbert, P. W., 1983, MNRAS, 204, 1269

Soltan, A., 1982, MNRAS, 200, 115-222

Trinchieri, G., Fabbiano, G., Canizares, C. R., 1986, ApJ, 310, 637-659

van der Marel, R., 1995a, MNRAS, 274, 884-898 van der Marel, 1995b, in New Light on Galaxy Evolution, (ed. Bender, R., & Davies, R. L.), IAU Symp. No. 171, Kluwer, Heidelberg.

Wandel, A., & Mushotzky, R. F., 1986, ApJ, 306, L61-L66

Wrobel, M. J., 1991, AJ, 101, 127-147

Figure Captions

Figure 1: The spectrum produced by an advection–dominated disk with $\alpha = 0.3$, $\beta = 0.5$, $m = 5 \times 10^9$, and $\dot{m} = (3, 6, 12, 24) \times 10^{-4}$. The plots are calculated numerically by the method described in §5.1.1.. The three labels correspond to the three cooling processes: synchrotron cooling (S), Compton cooling (C), and bremsstrahlung cooling (B). ν_p and $\nu_{\min}$ correspond to the radio frequencies from the region $3 \le r \le 10^3$.

Figure 2: The equilibrium temperatures as a function of $\dot{m}$, for different values of m, and the corresponding values of x_M. For low $\dot{m}$, $\delta\, Q^+$ dominates the heating of the electrons.

Figure 3: Plot of $1 - \alpha_c$ as a function of $\dot{m}$ for the corresponding plots in Fig. 2.

Figure 4: Plot of $L_{\rm ADAF}/L_{\rm Edd}$ as a function of $\dot{m}$ for different values of α. The plot can be used for any value of m (see text).

Figure 5: Spectra for $m = (0.5, 5, 10, 30) \times 10^8$, and their corresponding $\dot{m}$ given by eq.(56). The bar and arrow represent the 0.2 – 4 keV upper bounds for the x-ray core emission from the bright elliptical galaxies given in Table 2. The upper bounds in the radio are the unresolved compact core fluxes (Wrobel 1991).

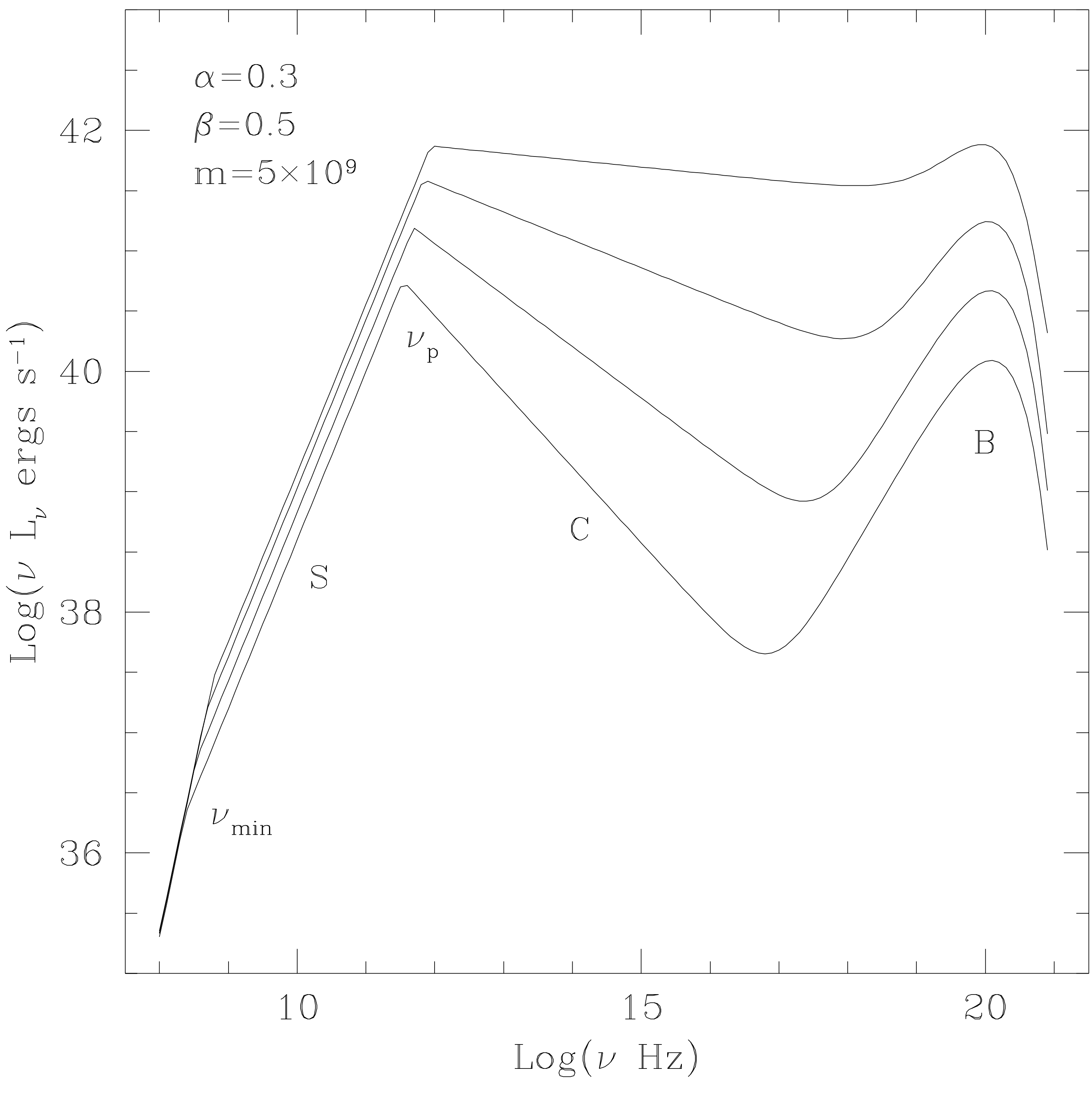

α=0.3
β=0.5
m=5×10⁹
Log(ν L_ν ergs s⁻¹)
Log(ν Hz)
ν_p
ν_min
S
C
B
42
40
38
36
10
15
20

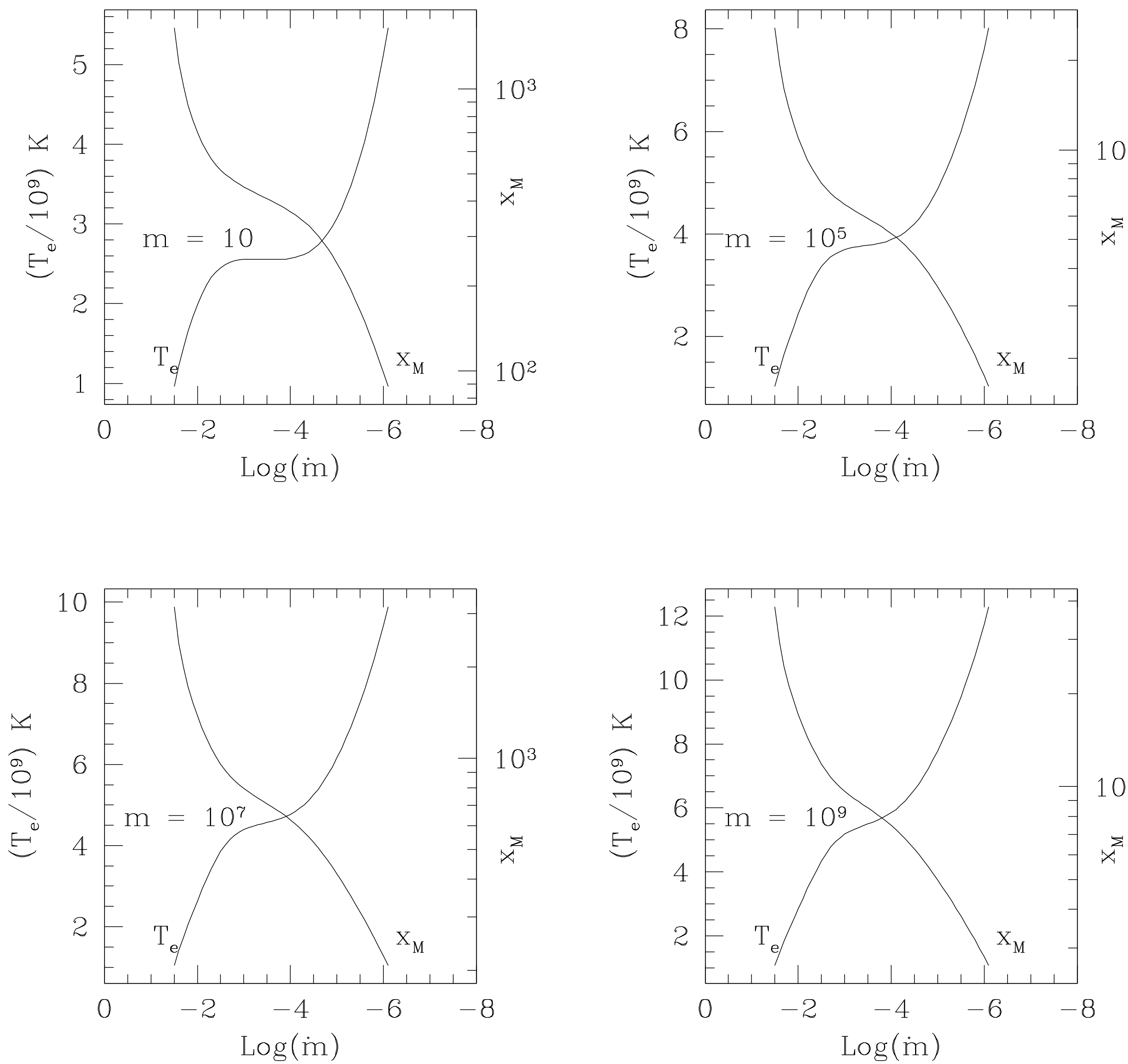

m = 10
m = 10^5
m = 10^7
m = 10^9
(T_e/10^9) K
x_M
T_e
Log(ṁ)
10^3
10^2

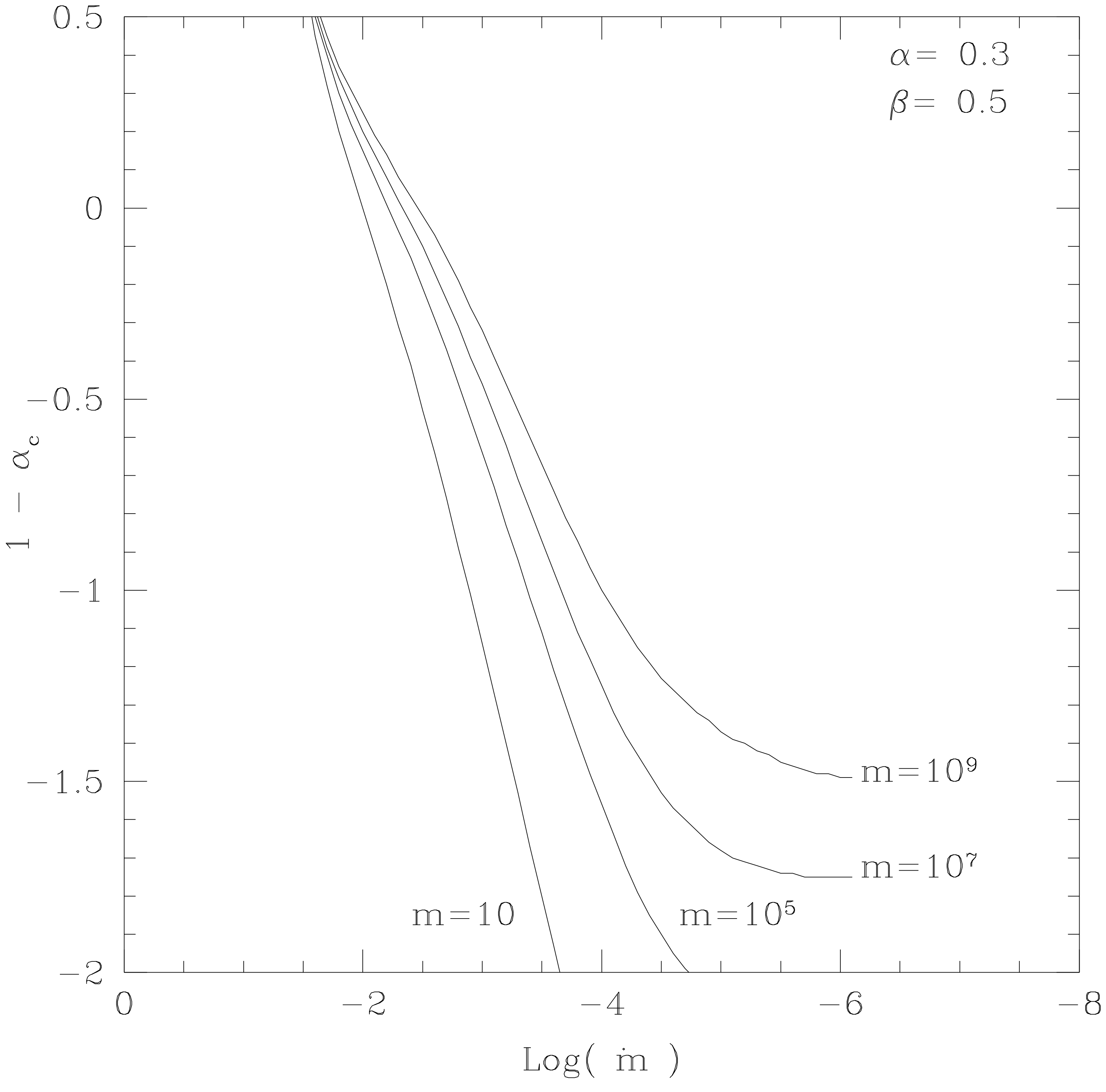

$\alpha = 0.3$
$\beta = 0.5$
$m=10^9$
$m=10^7$
$m=10^5$
$m=10$
0.5
0
−0.5
−1
−1.5
−2
0
−2
−4
−6
−8
$1 - \alpha_c$
Log($\dot{m}$)

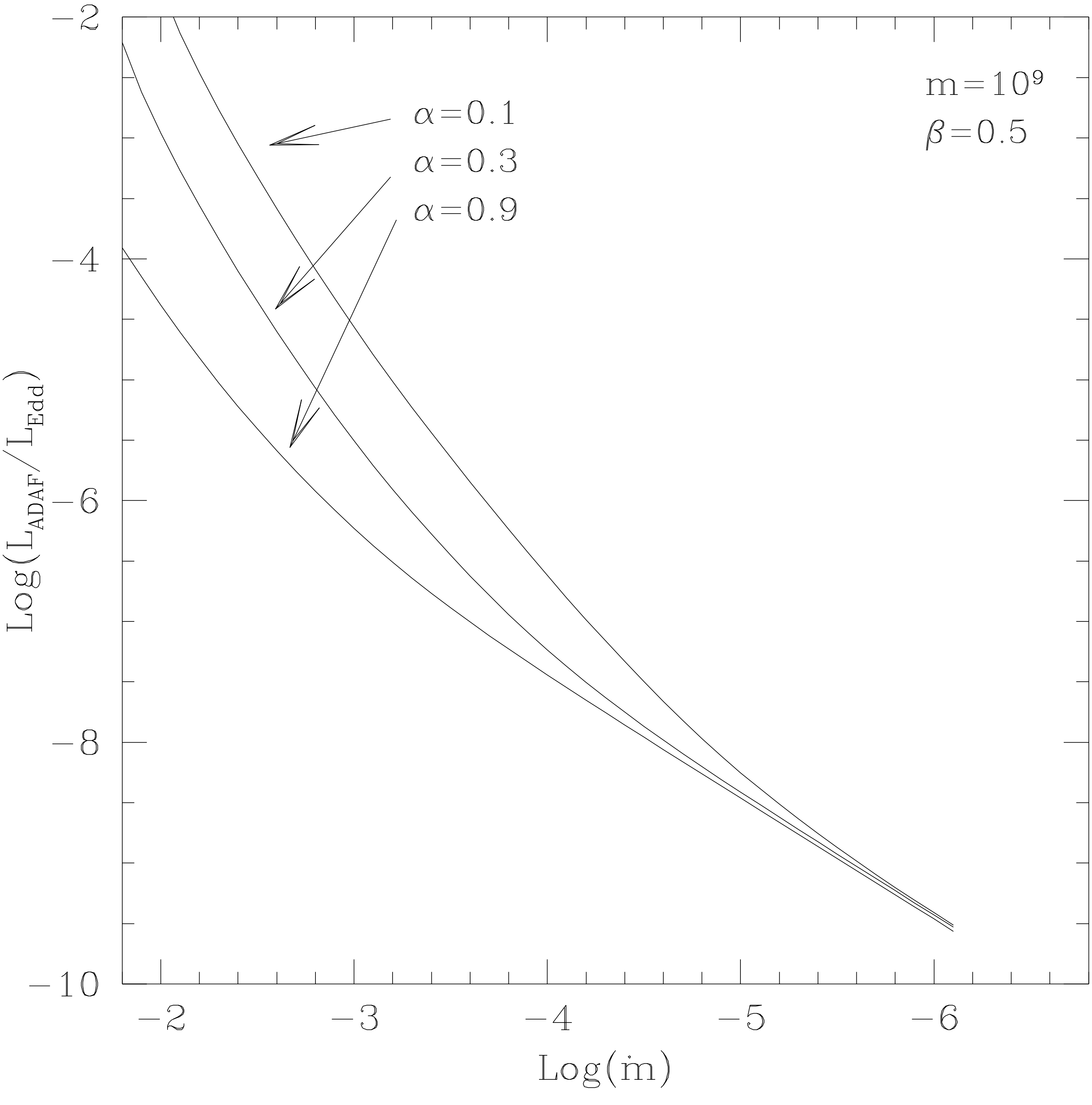

m=10⁹
β=0.5
α=0.1
α=0.3
α=0.9
−2
−4
−6
−8
−10
Log(L_ADAF/L_Edd)
−2
−3
−4
−5
−6
Log(ṁ)

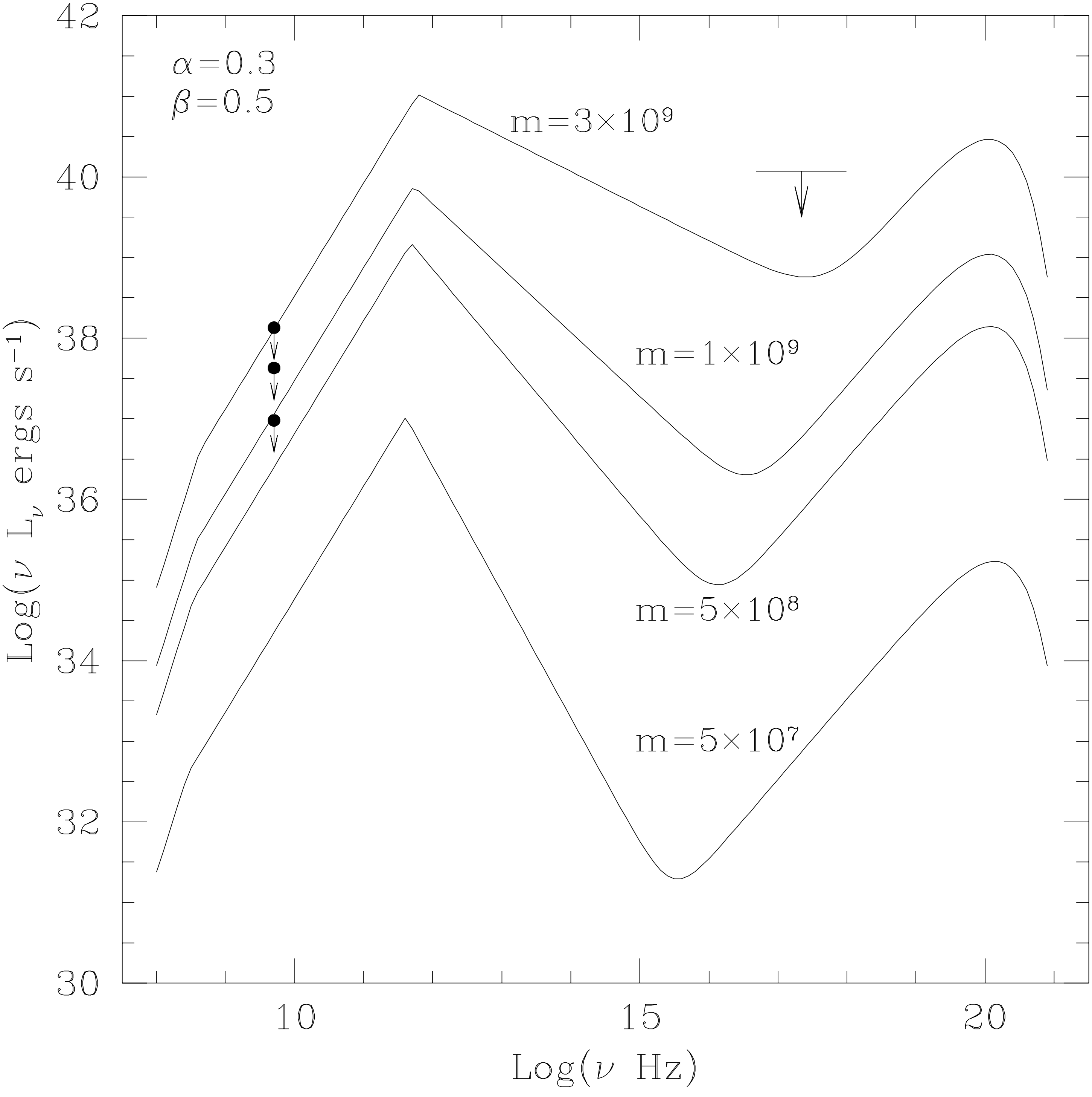
α=0.3
β=0.5
m=3×10⁹
m=1×10⁹
m=5×10⁸
m=5×10⁷
Log(ν L_ν ergs s⁻¹)
Log(ν Hz)
42
40
38
36
34
32
30
10
15
20